Investigation of the Influence of Cation/Anion Ratio on the Structure and Magnetism of $La_xCr_yO_3$

by

Su Muqing

B.Sc. in Applied Physics and Chemistry

2023/2024

Faculty of Science and Technology

University of Macau

Investigation of the Influence of Cation/Anion Ratio on the Structure and Magnetism of $La_xCr_yO_3$

by

Su Muqing (DC027658)

Final Year Project Report submitted in fulfillment of
the requirements for the degree of

BSc. in Applied Physics and Chemistry

Project Supervisor
Haifeng Li

Faculty of Science and Technology
University of Macau

2023/2024

ABSTRACT

Structural and magnetic properties of $LaCrO_3$, $La_{0.95}CrO_3$, $La_{1.05}CrO_3$, $LaCr_{0.95}O_3$ and $LaCr_{1.05}O_3$are reported in this work. These series of perovskite samples were prepared by combustion synthesis and were characterized by X-ray diffraction (XRD), physical property measurement system (PPMS) techniques to exam the effect of different doping level on La and Cr on physicochemical properties. Comparing with the original sample $LaCrO_3$ with a predominant antiferromagnetic phase transition near 295 K, others show an approximate but unequal value due to the structural changes. Investigated by Rietveld analysis, we observed this change which will affect the distortion angle of the CrO_6 octahedral to further influence the magnetic structure and causes the shifting of magnetic conversion temperature.

TABLE OF CONTENTS

LIST OF FIGURES

Number *Page*

LIST OF TABLES

Number *Page*

ACKNOWLEDGMENTS

I wishes to express my gratitude to all the members of Mr. Li's research group, without whose effort I can't successfully complete this article. Take this opportunity, I would like to highlight two of these members for their contributions to this article.

First, the highest expression of gratitude is dedicated to my teacher Prof. Haifeng Li. I am grateful to you for opening the doors of the laboratory to me and provided me with the opportunity to experience the joy and challenges of scientific experimentation. At the same time, I would also like to thank you for taking the time to personally trained me and gave me your comments on the article. I will keep your teachings in mind and use them in my future studies.

I would also like to thank Miss Kaitong Sun who guided me into the laboratory and instructed me in various experiment. It was her carefulness and dedication that influenced me in many ways and laid a solid foundation for my future studies and career path. What's more, she also taught me how to analysis experiment data, drawing any kinds of figure and write a good article. Here I want to express my gratitude to her for her diligent teaching and patient guidance.

It is an honor for me to join Mr. Li's research group. I will definitely continue to work hard to live up to expectations.

CHAPTER 1: INTRODUCTION

Transition metal oxides have become very attractive materials for researchers, especially the perovskite type oxide compounds, has got more and more attention in the field of material physics and chemistry due to its elusive and changeable magnetic properties [1]. A number of these complex oxides, which have a perovskite structure, exhibit diverse magnetic properties not only in the form of bulk samples [2] but also as single crystals [3]. Among them, chromium compound was fascinating rely on their intriguing magnetic and ferroelectric properties. Due to the interaction between 4f and 3d orbitals, their magnetic properties are complex. The presence of t-e orbital hybridization [4], distortion of oxygen octahedron [5] and Cr^{3+}-O-Cr^{3+} super-exchange interaction makes the reasons confusing.

Back to 1950s, Koehler has begun to investigate some magnetic properties of magnetic perovskite compounds whose A-site is Lanthanum [6]. Some relevant research also focuses on $LaCrO_3$, such as Zhou's study on the magnetic structure of $LaCrO_3$ under High Pressure from In situ neutron diffraction [7]. According to Fig 1 graphed by VESTA [8], $LaCrO_3$, a G-type distorted perovskite material, has been considered as having an orthorhombic crystal structure with the space group Pnma [9]. Due to the deflection of the CrO_6 octahedron, the conventional Cr-O-Cr angle deviates from the 160 degrees of the ideal perovskite, which in turn causes the internal structure of $LaCrO_3$ to be distorted. Furthermore, due to the corresponding changes in the crystal field effect and super-exchange effect, the magnetic properties of $LaCrO_3$ will also change. Recently there's also

a lot of studies based on the influence of doping transition metal have published, like Ir doped $LaCrO_3$ [10] and Al half-doped $LaCrO_3$ [11].

In this study, a series of $LaCrO_3$ polycrystalline powder with different doping level on lanthanum and chromium, respectively, were synthesized using solid-state reaction method. The effect of different doping level onto the magnetic conversion temperature was also investigated and compare them together.

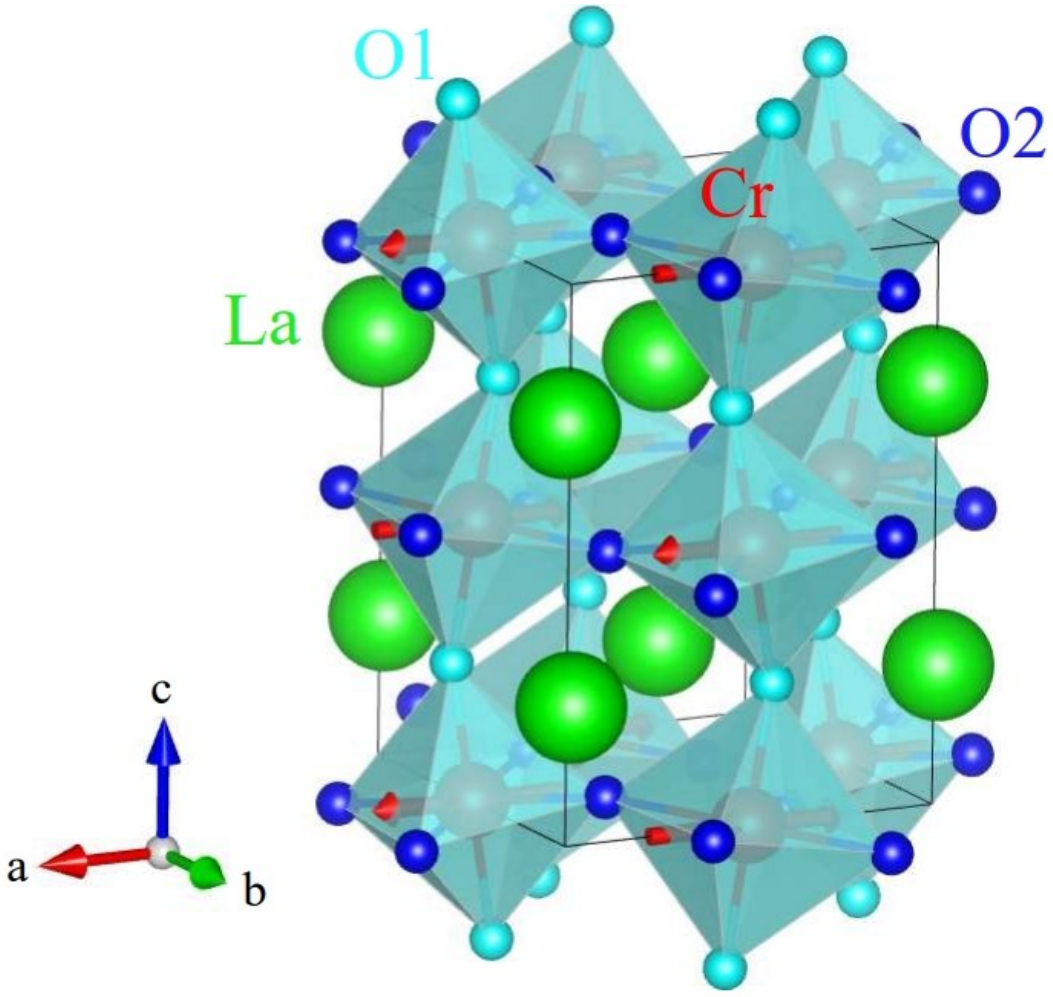

(Fig 1. Orthorhombic crystal structure (with space group Pnma) with one unit cell (solid lines) of $LaCrO_3$ and the AFM structure in one AFM unit cell. The arrows on the Cr ions indicate the spins of chromium atom.)

CHAPTER 2: EXPERIMENTAL

We prepare our polycrystalline samples strictly using stoichiometric mixtures of raw La_2O_3 (ALFA AESAR, 99.9%) and Cr_2O_3 (ALFA AESAR, 99.6%) compounds, preparing La_2O_3 and Cr_2O_3 powders respectively in the ratio of x to y, through the traditional solid-state reaction method which was done by a box furnace [12], to get our sample $La_xCr_yO_3$. After being milled and mixed using a Vibratory Micro Mill, the sample was heated in air to 1000°C at a rate of 180°C/h to facilitate the prereaction process to remove moister and to make sure the two ingredients are well mixed [13]. Two another similar heating procedure was conducted at 1100°C and 1200℃, respectively, in order to make sure the sample was well-prepared. At the same time, we also observed that some samples changed color from green to yellow-brown during the sintering process. This may be due to the generation of La and O defects in the crystal lattice [14]. Powder X-ray diffraction (XRD) data were acquired using a diffractometer at room temperature using a Cu-α radiation tube operating at 45 kV and 200 mA. XRD data were performed in step scanning mode in the range of 10–90° (2θ) with a step size of 20° and a scanning speed of 20°/min. The structural analysis system (FULLPROF) software was used to perform Rietveld refinement of the diffraction pattern and extract the structural parameters. The Bragg peak is modeled using the pseudo-Voigt function, and the background is estimated using polynomial background modeling. We measured the magnetization of the $LaCrO_3$ samples using a Quantum Design physical property measurement system (PPMS DynaCool instrument). The dc magnetization measurements were conducted at an applied magnetic field of 0.01 T using two modes: the

zero-field cooling (ZFC) mode and the field-cooling (FC) mode. The measurements were performed in the temperature range of 1 to 399 K. The magnetic transition temperature can be found computationally by calculating the magnetic susceptibility and plotting the magnetic susceptibility temperature curve.

CHAPTER 3: RESULTS AND DISCUSSION

SECTION1 XRD data analysis

Figure 2 shows the Rietveld-refined X-ray diffraction (XRD) pattern of the $La_xCr_yO_3$ series samples (Fig. 2(a~e)) and the comparison diagram of all data (Fig. 2f). The distribution of differences between observed and calculated diffraction patterns is shown at the bottom of the figure. The R factors Rp, Rwp and Rexp all show small values, and χ obtains a good fit (none are greater than 4). The lattice constant and volume of the unit cell a are distributed around 5.517A, b is distributed around 5.478A and c is distributed around 7.760A. The obtained volumes are also around 234.6A2. This is within the acceptable range of early reports [15]. The XRD comparison chart can also reflect that our series of $La_xCr_yO_3$ materials have roughly the same peak shape and crystal phase as pure $LaCrO_3$, and since our samples are prepared uniformly, this basically verifies the accuracy of our materials.

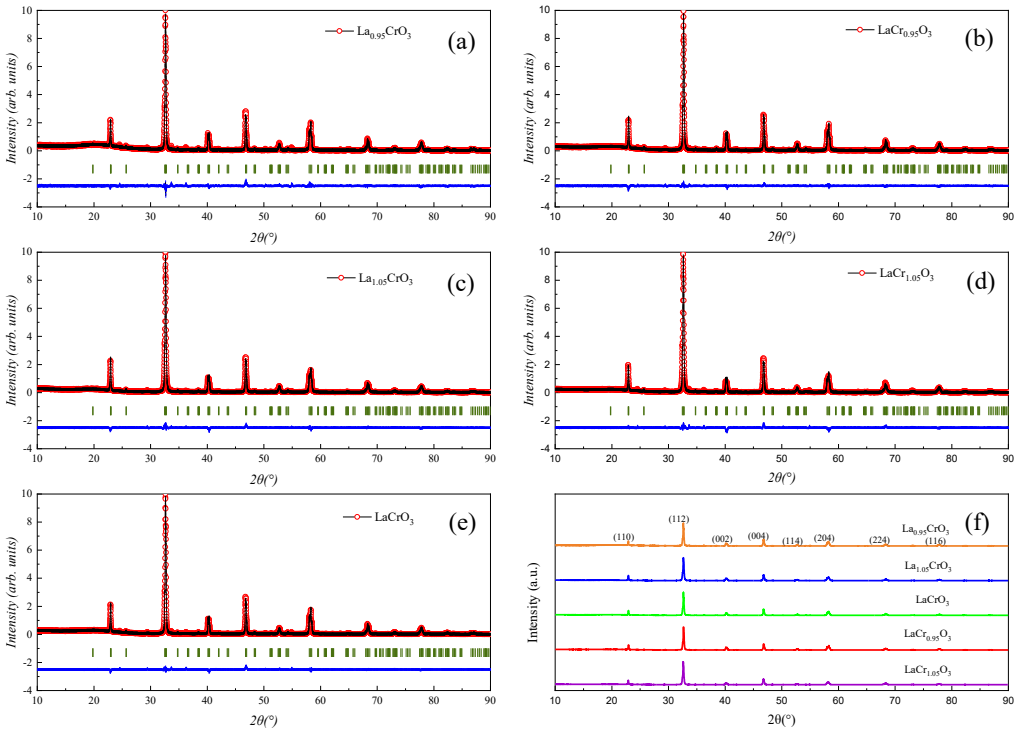

(Fig 2. Observed (circles) and calculated (solid lines) XRD patterns for $LaCrO_3$ series sample The vertical bars mark the positions of Bragg reflections (space group Pnma) , and the lower curves represent the difference between observed and calculated patterns a) $La_{0.95}CrO_3$, b) $LaCr_{0.95}O_3$, c)$La_{1.05}CrO_3$ d) $LaCr_{1.05}O_3$, e) $LaCrO_3$, f) $LaCrO_3$ series sample data with plans)

SECTION2 Magnetization versus temperature

Figure 3 shows magnetization measurements of a small amount of $LaCrO_3$ series polycrystalline sample. The unit of vertical axis has been transformed into μB per Cr^{3+} ion which may help to illustrate the magnetic induction of a single chromium atom. According to Fig. 3(a), we can find that there is a significant difference between the FC curve and the ZFC curve below about 290°C. In the case of an external magnetic field (FC), the samples of the $La_xCr_yO_3$ series compounds all show a low degree of magnetization at high temperatures but significantly increase to a fixed value after cooling down above the

magnetic transition temperature point which nearly makes its magnet value quadrupled in 30K. In the absence of an external magnetic field (ZFC), the magnetic induction intensity of Cr ions does not show much change with temperature changes, but only shows a slight increase near the magnetic transition point temperature due to the spontaneous magnetization effect. There is not much difference between the two above the magnetic switching temperature. The above phenomenon perfectly proves that $LaCrO_3$ is a paramagnet above the magnetic transition temperature and a G-type antiferromagnet below the magnetic transition temperature and rules out the possibility for a ferrimagnet, which fit well with Brajesh's work [16]. This magnetic transition temperature should be regarded as the Neel temperature.

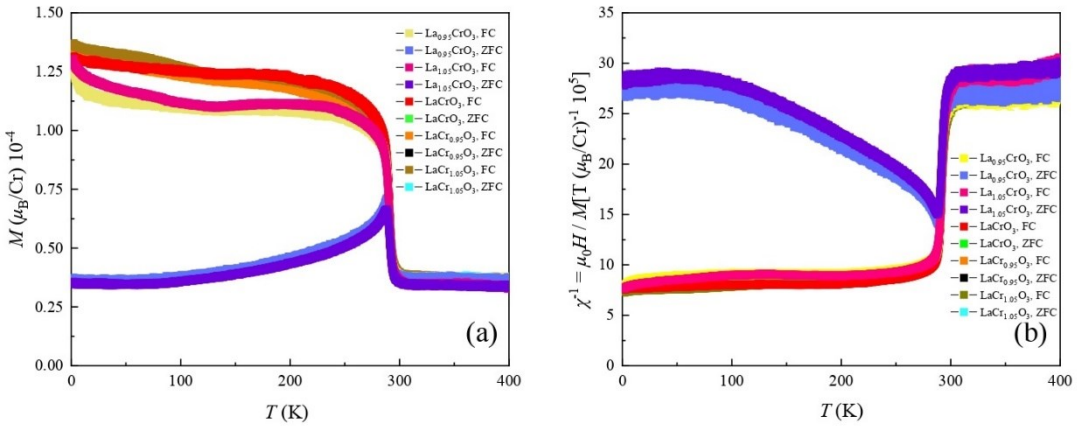

(Fig 3. (a) The magnetization (M) of chromium ions in the $La_xCr_yO_3$ series compounds, measured at μ0H = 0.01 T, is presented as a function of temperature for both ZFC and FC.
(b) The inverse magnetic susceptibility χ−1 (circles) of chromium ions in the LaxCryO3 series compounds is plotted against temperature for both ZFC and FC. The color of the curve in the figure represents the type of compound and detection method. The fit results are listed in Table I.)

We also calculated the inverse magnetic susceptibility χ−1 = μ0H/M as shown in Fig. 3(b), and we found that the paramagnet of $LaCrO_3$ exhibits a phenomenon that does not comply with the CW law in the range from the magnetic transition temperature to room temperature.

Only by doing more $LaCrO_3$ experiments at high temperatures can further conclusions be drawn.

SECTION3 Magnetic transition temperature

The study of magnetic transition points is crucial to understanding and applying magnetic materials. It provides important information about magnetic moment interactions, spin structure, and magnetic phase transition mechanisms in materials. The accurate positioning and understanding of magnetic transition points can help us design and optimize the application of magnetic materials in magnetic storage, sensors, magnetic sensors and other fields [17]. We successfully found the magnetic transition temperature point of the $La_xCr_yO_3$ series samples and the results were accurate to a certain point, listed in Fig 4(a~e). First, we selected an approximate temperature value range. In order to reduce errors, we selected this temperature range from 280K to 310K, and extracted the FC value of this interval for each sample. We first used a derivation to determine the temperature point at which the inclination angle is maximum but we failed since we had many measured data points. So we fitted the curve after the first derivation with Gaussian, and then performed a second derivation on the fitted result, so as to accurately find which point has the largest change, so as to determine the magnetic transition point value of our sample. Table 1 below has listed all the data we collect. We can clearly find that the magnetic deflection temperature of the two samples that changed the number of chromium atoms is significantly lower than the other three samples, with an average reduction of about two degrees. The

performance of the sample with changed lanthanum coordination number is not much different from that of the prepared ordinary $LaCrO_3$ sample.

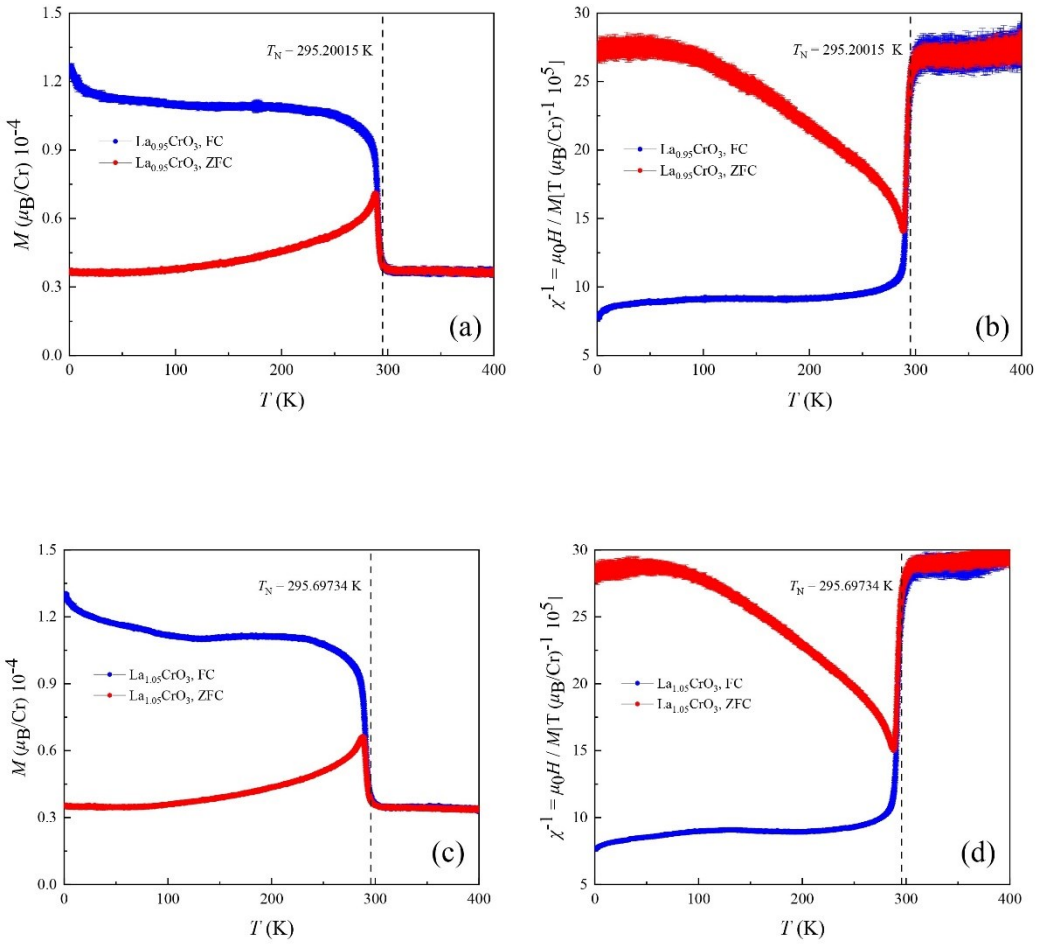

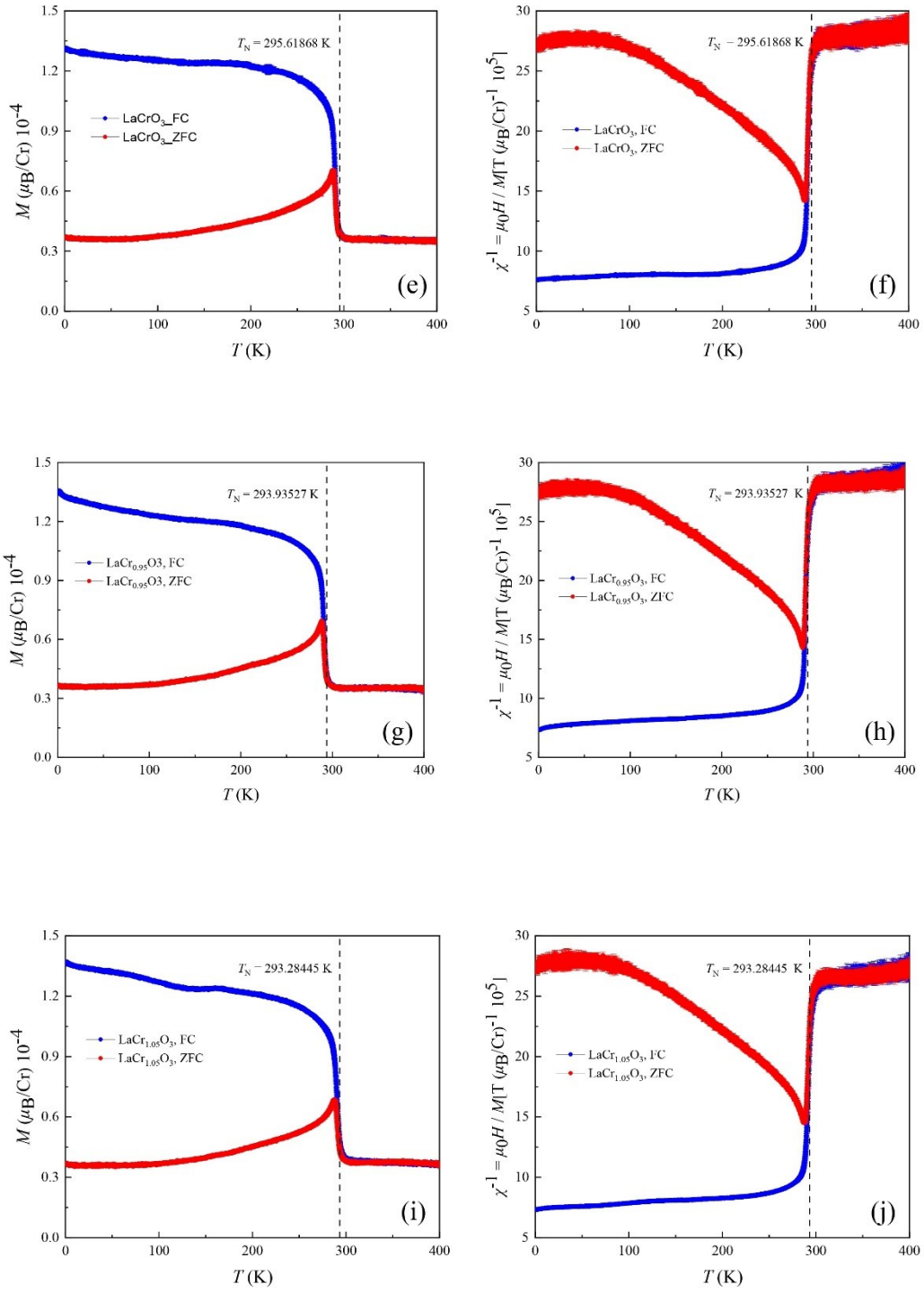

(Fig 4. (a~e) The magnetization (M) of chromium ions in $La_xCr_yO_3$ series compounds were measured as a function of temperature at 0.01T, and both zero-field-cooled (ZFC) and field-cooled (FC) values were obtained. (b) The inverse magnetic susceptibility χ^{-1} of chromium ions in $La_xCr_yO_3$ series compounds were also measured as a function of temperature, and the corresponding ZFC and FC values were plotted. The dash-dotted line indicates the analyzed Neel temperature.)

	$La_{0.95}CrO_3$	$La_{1.05}CrO_3$	$LaCrO_3$	$LaCr_{0.95}O_3$	$LaCr_{1.05}O_3$
T_N (K)	295.20015	295.69734	295.61868	293.93527	293.28445

(Table 1: Nair temperature of the compiled $LaCrO_3$ series samples)

SECTION4 Local distortion modes for La, Cr and O ions

Determining the detailed local crystal environment is essential for determining the electronic structure, spin configuration, orbital degeneracy and crystal field effects of 3d, 4d, 5d or 4f-compounds [18]. In order to further analyze the relationship between atomic structure and magnetism and quantitatively measure the local crystal environment, we use the following formula to calculate the distortion parameters of each atom [19]:

$$\Delta = \frac{1}{n}\sum_{i=1}^{n}\left(\frac{d_n - \langle d\rangle}{\langle d\rangle}\right)^2,$$

where n is the coordination number, dn is the bond length along one of the coordination directions, and d is the average bond length. Through this formula, we calculated the local distortion parameters of ions in a series of $La_xCr_yO_3$ samples. As shown in Table 2, we list the calculated distortion parameters for all ions. Among them, we mainly focus on the distortion parameters of Cr to explore the impact of oxygen octahedral deflection on the magnetic characteristics of the sample. Figure 5 shows a $LaCrO_3$ unit cell after removing the remaining atoms, leaving only the chromium octahedron and its coordination with oxygen atoms. We can more intuitively observe the influence of the bond length of Cr-O1

and Cr-O2 and the angle between Cr-O1-Cr and Cr-O2-Cr on the declination angle between oxygen octahedrons.

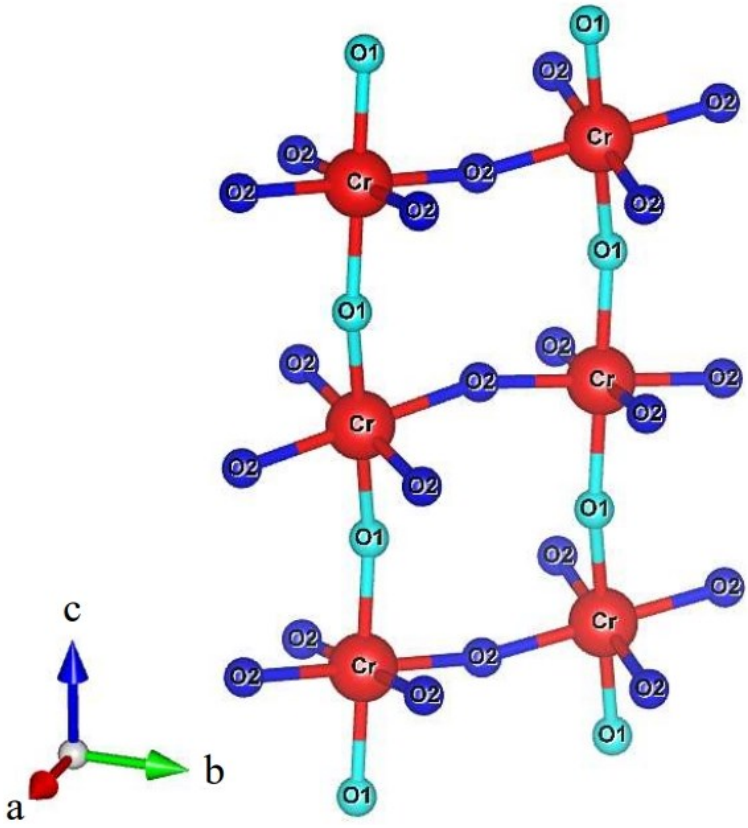

(Fig 5. A simplified diagram of the coordination diagram of six chromium ions and oxygen ions selected in the $LaCrO_3$ unit cell, the connection method of Cr-O1 and Cr-O2 and the influence of the angle on the distortion of the oxygen octahedron)

	$La_{0.95}CrO_3$	$La_{1.05}CrO_3$	$LaCrO_3$	$LaCr_{0.95}O_3$	$LaCr_{1.05}O_3$
a(Å)	5.5185(2)	5.5191(1)	5.5171(1)	5.5182(1)	5.5174(2)
b(Å)	5.4799(2)	5.4784(1)	5.4791(1)	5.4796(1)	5.4771(2)
c(Å)	7.7609(3)	7.7608(2)	7.7697(2)	7.7608(2)	7.7589(3)
$\alpha(\beta,\gamma)(^\circ)$	90	90	90	90	90
$V(Å^3)$	234.69(1)	234.66(1)	234.564(9)	234.666(8)	234.48(2)
La(4c)x	0.9968(5)	0.9963(3)	0.9962(4)	0.9964(3)	0.9918(4)
La(4c)y	0.0172(2)	0.0174(1)	0.0175(2)	0.0179(1)	0.0161(2)
La(4c)z	0.25	0.25	0.25	0.25	0.25
La(4c) $B(Å^2)$	1.58(5)	1.99(2)	1.44(3)	1.41(2)	2.03(3)
Cr(4b) (x,y,z)	(0.5,0,0)	(0.5,0,0)	(0.5,0,0)	(0.5,0,0)	(0.5,0,0)
Cr(4b) $B(Å^2)$	1.64(7)	1.27(4)	0.90(4)	0.66(4)	1.42(5)
O1(4c)x	0.058(3)	0.060(2)	0.059(2)	0.059(2)	0.020(5)
O1(4c)y	0.498(2)	0.491(1)	0.500(2)	0.494(1)	0.497(2)
O1(4c)z	0.25	0.25	0.25	0.25	0.25
O1(4c) $B(Å^2)$	1.0(1)	1.6(1)	1.0(1)	1.3(1)	1.8(2)
O2(8d)x	0.728(3)	0.731(2)	0.730(2)	0.729(2)	0.783(2)
O2(8d)y	0.272(3)	0.259(3)	0.262(3)	0.27(2)	0.286(2)
O2(8d)z	0.037(1)	0.031(1)	0.031(1)	0.034(1)	-0.015(2)
O2(8d) $B(Å^2)$	1.0(1)	1.6(1)	1.0(1)	1.3(1)	1.8(2)
La-O11(Å)	2.46(2)	2.45(1)	2.46(1)	2.46(1)	2.64(1)
La-O12(Å)	2.66(1)	2.618(8)	2.667(8)	2.634(8)	2.70(3)
La-O21(Å)(×2)	2.47(1)	2.55(1)	2.53(1)	2.49(1)	2.66(1)
La-O22(Å)(×2)	2.62(2)	2.61(1)	2.61(1)	2.63(1)	2.76(1)
⟨ La-O ⟩	2.549(6)	2.563(5)	2.568(5)	2.554(4)	2.696(7)
Cr-O1(Å)(× 2)	1.966(3)	1.969(2)	1.967(2)	1.968(2)	1.943(2)
Cr-O21(Å)(× 2)	1.97(2)	1.92(1)	1.93(1)	1.97(1)	1.68(1)
Cr-O22(Å)(× 2)	1.97(2)	2.00(1)	2.00(1)	1.97(1)	2.22(1)
⟨ Cr-O ⟩	1.971(6)	1.964(5)	1.964(5)	1.978(3)	1.946(4)
∠Cr-O1-Cr(°)	161.3(1)	160.42(8)	160.95(8)	160.77(8)	173.43(7)
∠Cr-O1-Cr(°)	160.5(7)	164.7(6)	164.0(6)	162.0(4)	173.0(5)
$\triangle(La)(\times10^{-4})$	11.472	4.969	7.484	8.901	3.027
$\triangle(Cr)(\times10^{-4})$	0.025	2.706	1.742	0.021	126.141
$\triangle(O1)(\times10^{-4})$	180.272	165.040	183.246	171.121	248.243
$\triangle(O2)(\times10^{-4})$	166.544	185.688	182.818	174.241	336.375
R_p	8.31	6.71	6.26	6.22	9.26
R_{wp}	13.7	10.0	11.0	9.84	15.1
R_{exp}	7.31	8.2	8.24	8.01	8.6
χ^2	3.54	1.5	1.77	1.51	3.07

(Table 2. By using the FULLPROF SUITE, the structural parameters of $La_{0.95}CrO_3$, $La_{1.05}CrO_3$, $LaCr_{0.95}O_3$, $LaCr_{1.05}O_3$ and $LaCrO_3$ at room temperature are refined, including lattice constant, unit cell volume, atomic position, isotropic thermal parameter (B), bond length, Bond angles, distortion parameters and fit. The number in parentheses is the estimated standard deviation to the last significant digit.)

By comparing the relationship between the oxygen octahedral deflection angle and the magnetic conversion temperature, we can find that among the five samples, excluding the measurement error of $LaCr_{1.05}O_3$, the oxygen octahedral distortion of $La_{1.05}CrO_3$ is the largest, with a value of 2.706×10^{-4}, and has the largest Nel temperature of 295.69734K. It is followed by $LaCrO_3$ with a distortion degree of 1.742×10^{-4} and a Nel temperature of 295.61868K. It is followed by $La_{0.95}CrO_3$ with a distortion degree of 0.0025×10^{-4} and a Nel temperature of 295.20015. Finally, $LaCr_{0.95}O_3$ has a distortion degree of 0.0021×10^{-4} and a Neel temperature of 293.93257K. It is not difficult to speculate that as the distortion of the oxygen octahedron decreases, the magnetic transition temperature of $LaCrO_3$ transforms from a paramagnet to a G-type antiferromagnet, also the Nair temperature is dropping. Moreover, compared with changing the coordination number of Cr, when changing the coordination number of La, the change in magnetic transition temperature is relatively smaller, which also shows that when changing the coordination number of Cr, the change in the number of Cr ions has an impact on the overall magnetic field. The impact of structure is huge. For the three samples that change the La coordination number, the increase in the La coordination number obviously reduces the degree of distortion of the oxygen octahedron, thereby increasing the magnetic transition temperature. The specific influence mechanism may require more subsequent magnetic detection experiments on $LaCrO_3$ samples with different coordination ratios of La to further explore.

CHAPTER 4: Conclusion

We prepared a series of $La_xCr_yO_3$ samples by solid-state sintering method, further confirmed the nature of the material by comparing XRD images, and conducted FC and ZFC tests on these samples respectively. By performing Rietveld refining on the data, calculating the degree of oxygen octahedral distortion, and comparing and analyzing the obtained magnetic transition temperatures, we summarized the shift in Neel temperature of $La_xCr_yO_3$ samples with different La and Cr ion coordination numbers. The increase in the coordination number of La atoms in the material leads to an increase in the degree of oxygen octahedral distortion, and shows an increase in the Neel temperature of the corresponding material. The reduction in the coordination number of Cr atoms leads to a reduction in distortion and a slightly larger reduction in Neel temperature. More experiments should be done to explore more patterns.

REFERENCES

[1] Ramadass, N. (1978a) 'Abo3-type oxides—their structure and properties—a bird's Eye View', *Materials Science and Engineering*, 36(2), pp. 231–239. doi:10.1016/0025-5416(78)90076-9.

[2] Zhu, Y. *et al.* (2020) 'High-temperature magnetism and crystallography of a ', *Physical Review B*, 101(1). doi:10.1103/physrevb.101.014114.

[3] Tiwari, B. *et al.* (2015) 'Magnetostructural and magnetocaloric properties of bulk lacro3system', *Materials Research Express*, 2(2), p. 026103. doi:10.1088/2053-1591/2/2/026103.

[4] Zhu, Y. *et al.* (2022) 'Crystal Growth Engineering and origin of the weak ferromagnetism in antiferromagnetic matrix of orthochromates from T-e orbital hybridization', *iScience*, 25(4), p. 104111. doi:10.1016/j.isci.2022.104111.

[5] Hong, Y. *et al.* (2021) 'Local-electrostatics-induced oxygen octahedral distortion in perovskite oxides and insight into the structure of Ruddlesden–Popper Phases', *Nature Communications*, 12(1). doi:10.1038/s41467-021-25889-6.

[6] Koehler, W.C. and Wollan, E.O. (1957) 'Neutron-diffraction study of the magnetic properties of perovskite-like compounds labo3', *Journal of Physics and Chemistry of Solids*, 2(2), pp. 100–106. doi:10.1016/0022-3697(57)90095-1.

[7] Zhou, J.-S. *et al.* (2011) 'Magnetic structure of LaCrO3 Perovskite under High Pressure from *In Situ* Neutron Diffraction', *Physical Review Letters*, 106(5). doi:10.1103/physrevlett.106.057201.

[8] Momma, K. and Izumi, F. (2008) '*vesta*: A three-dimensional visualization system for electronic and structural analysis', *Journal of Applied Crystallography*, 41(3), pp. 653–658. doi:10.1107/s0021889808012016.

[9] Oikawa, K. *et al.* (2000) 'Structural phase transition of orthorhombic LaCrO3 studied by neutron powder diffraction', *Journal of Solid State Chemistry*, 154(2), pp. 524–529. doi:10.1006/jssc.2000.8873.

[10] Coşkun, M. *et al.* (2018) 'Frequency and temperature dependent electrical and dielectric properties of LaCrO3 and IR doped LaCrO3 perovskite compounds', *Journal of Alloys and Compounds*, 740, pp. 1012–1023. doi:10.1016/j.jallcom.2018.01.022.

[11] Silva, R.S. *et al.* (2016) 'Structural and magnetic properties of lacro 3 half-doped with al', *Ceramics International*, 42(13), pp. 14499–14504. doi:10.1016/j.ceramint.2016.06.059.

[12] Li, H. (2008) *Synthesis of CMR manganites and ordering phenomena in complex transition metal oxides*. Ju¨lich, North Rhine-Westphalia: Forschungszentrum, Zentralbibliothek.

[13] Enhessari, M. *et al.* (2017) 'Kinetic properties and structural analysis of LaCrO3Nanoparticles', *Materials Science-Poland*, 35(2), pp. 368–373. doi:10.1515/msp-2017-0043.

[14] Ong, K.P., Blaha, P. and Wu, P. (2008) 'Origin of the light green color and electronic ground state of LaCrO3', *Physical Review B*, 77(7). doi:10.1103/physrevb.77.073102.

[15] Tiwari, B., Rao, M.S.R. and Dixit, A. (2012) 'Ground state electronic and magnetic properties of lacro3 system', *Advanced Materials Research*, 585, pp. 274–278. doi:10.4028/www.scientific.net/amr.585.274.

[16] Tiwari, B., Dixit, A. and Ramachandra Rao, M.S. (2020) 'Anomalous magnetic behavior and complex magnetic structure of proximate lacro3—lafeo3 system', *Materials Research Express*, 6(12), p. 126119. doi:10.1088/2053-1591/ab6535.

[17] Rivero, G., Spottorno, J. and Multigner, M. (2012) *Magnetic sensors for biomedical applications*. Hoboken, New Jersey: INTECH Open Access Publisher.

[18] Li, H. (2008) *Synthesis of CMR manganites and ordering phenomena in complex transition metal oxides*. Ju¨lich, North Rhine-Westphalia: Forschungszentrum, Zentralbibliothek.

[19] Li, H.-F. *et al.* (2009) 'Crystal and magnetic structure of single-crystal LA1-x SR x MnO 3 (x ≈ 1/8)', *The European Physical Journal B*, 67(2), pp. 149–157. doi:10.1140/epjb/e2009-00019-5.